

Imaging studies of crystalline arthritides

F. Paparo¹, E. Fabbro², G. Ferrero², R. Piccazzo², M. Revelli², D. Camellino³,
G. Garlaschi², M.A. Cimmino³

¹Department of Radiology, E.O. Ospedali Galliera, Genoa, Italy;

²Internal Medicine Department, Radiology Section, University of Genoa, Genoa, Italy;

³Internal Medicine Department, Rheumatology Clinic, University of Genoa, Genoa, Italy

SUMMARY

Gout, calcium pyrophosphate dihydrate (CPPD) deposition disease, and calcium hydroxyapatite deposition disease (HADD) are the three most common crystal-induced arthropathies. Multimodality imaging may help in their diagnosis, and is useful for a precise and comprehensive assessment and grading of the related osteoarticular damage. Plain film radiography, due to its low cost and wide availability, is the first imaging technique to be used in crystal deposition diseases, providing well-known and specific findings for CPPD deposition disease and HADD, while it may undergrade the early osteoarticular lesions in gouty patients. Ultrasonography (US) is a radiation-free approach that accurately depicts crystal deposits in cartilage, peri- and intra-articular soft tissues, but it does not give a panoramic view of the affected joints. Cross-sectional imaging techniques can examine crystal deposits in the spine and axial joints. CT has the potential to distinguish monosodium urate (MSU) crystals from calcium containing crystals, due to their different attenuation values. MRI may demonstrate synovitis, erosions and bone marrow edema in gouty patients and it may differentiate tophi from other soft tissue nodules due to its high contrast resolution and power of tissue characterization.

Key words: *gout, calcium pyrophosphate dihydrate deposition disease, calcium hydroxyapatite deposition disease, crystal-induced arthritides, dual-energy CT.*

Reumatismo, 2011; 63 (4): 263-275

■ INTRODUCTION

The three most common types of crystal-induced arthropathy are gout, calcium pyrophosphate dihydrate (CPPD) deposition disease, and calcium hydroxyapatite deposition disease (HADD) (1, 2). Their diagnosis is based on clinical presentation and laboratory findings, with the gold standard represented by demonstration of crystals in the joint synovial fluid by polarizing light microscopy (2-4).

In gout, imaging findings may vary in relation to the clinical phase (i.e. asymptomatic hyperuricemia, acute gouty arthritis, inter-critical gout and chronic tophaceous gout), playing an important role in the assessment and grading of disease-related osteo-articular damage and its progression both over time and in response to urate-lowering therapies. Imaging may also help to demonstrate MSU deposits and disease-related lesions in rare sites of involvement, such as spine and sacro-iliac joints) (2, 5).

Radiography remains the most commonly used imaging technique in the initial evaluation of gout (6). Computed tomography may detect cortical bone erosions with sensitivity superior to that of radiography, and it may demonstrate MSU deposits within tophi due to their specific attenuation value (7).

Magnetic resonance imaging has a high power for tissue-characterization and provides excellent contrast resolution which is improved by the intravenous administration of paramagnetic contrast material. It may provide information on the presence and grade of synovial thickening and hyperemia, synovial effusion and bone marrow edema (BME) which are the prominent features of the early stage of the disease (8, 9).

CPPD deposition disease is an inflammatory arthritis promoted by the deposition of calcium pyrophosphate dihydrate crystals within the synovium and peri-articular soft tissues, while the term chondrocalcinosis

Corresponding author:
Francesco Paparo, MD
Department of Radiology
E.O. Ospedali Galliera
Mura delle Cappuccine, 14
16128 Genoa, Italy
E-mail: francesco.paparo.ge@fastwebnet.it

sis refers to the radiographic evidence of calcification in hyaline and/or fibro-cartilage, either with or without accompanying symptoms (2, 3).

The gold-standard diagnosis of CPPD deposition disease relies on the demonstration of a typical X-ray diffraction pattern of crystals obtained from arthrocentesis, or when a radiographic polyarticular chondrocalcinosis is present and combined with the evidence of weakly birefringent crystals on polarizing light microscopy of the synovial fluid. Cross-sectional imaging studies (CT and MRI) are useful for a precise assessment of pyrophosphate arthropathy of the axial skeleton, in particular of the atlo-axial joint (i.e. "crowned dens" syndrome) (2, 3). In the case of periarticular HADD, which is mainly represented by calcific tendonitis of the shoulder, diagnosis principally relies on clinical presentation and imaging. This is considered a useful tool for monitoring the disease course over time and for guiding mini-invasive therapeutic procedures, such as ultrasonography-guided single or double needle lavage techniques and intra-articular injection of anti-inflammatory drugs.

In the rare case of intra-articular HADD, the gold standard for diagnosis is the demonstration of needle-like hydroxyapatite crystals on electron microscopy, identified as purple clumps by light microscopy with Wright's stain (10).

■ GOUT

Radiography

Plain film radiography is the first-line imaging tool used in the assessment of gouty patients, although in the early stage of the disease X-rays are usually normal or show non-specific findings (i.e. soft tissue swelling of the involved joint secondary to synovitis, capsular distention, and periarticular soft tissue edema) (6, 11). Plain X-ray features of chronic gout are well recognized and some of them (i.e. asymmetric periarticular soft tissue swelling or subcortical cysts without erosions) are included in the American College of Rheumatology

preliminary clinical diagnostic criteria for gout (12).

An attempt has been made by Dalbeth et al. (13) to adapt the Sharp/van der Heijde radiographic scoring system used in rheumatoid arthritis to gout (14). This modified system combines the additional scoring of distal interphalangeal joints of hands to the erosion and narrowing scoring of the other joints of hands and feet (wrist, interphalangeal, metacarpophalangeal, metatarsophalangeal, and interphalangeal joint of the great toe). This method has been shown to be an accurate and reliable tool for the assessment of joint damage in chronic gout. No additional benefit in terms of reliability or reproducibility has been demonstrated when additional features, such as extra-articular erosions, ankylosis or joint space widening, were added (13).

In the late stage of the disease, plain film X-ray shows asymmetric soft-tissue masses (tophi) close to punched-out, juxta-articular, eccentric erosive lesions that are associated with only minimal reactive new bone formation (Figure 1) (3, 6). In chronic tophaceous gout, tophaceous deposits can occur in the articular cartilage, subchondral bone, synovial membrane, and capsula, as well as in periarticular tissues such as tendons, ligaments, and bursae, particularly in the olecranon and prepatellar regions (3). Tophi are extracellular deposits of monosodium urate crystals (MSU) surrounded by foreign-body giant cells and mononuclear cells which form a granuloma-like structure (2). Tophaceous deposits may also mimic a space-occupying lesion, producing compression and impingement of nervous structures (e.g. carpal tunnel syndrome) (5, 6). Tophi apparently take years to develop during the course of gout, and they may on occasion be seen, in the absence of arthritis, as the initial manifestation of gout; a condition defined as "gout nodulosis" (9, 11).

A typical feature of gouty erosions is the overhanging edge, an elevated margin of bone that extends over the expected confines of the cortex at the site of erosion (15) which may represent new bone formation around a gradually enlarging tophus (Fig-

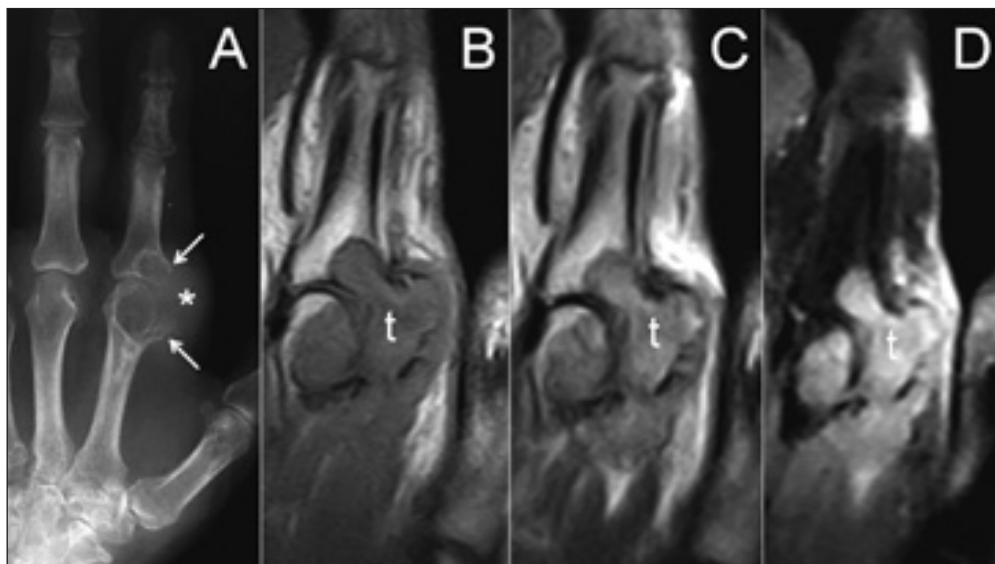


Figure 1 - The plain film X-ray (A) demonstrates asymmetric and nodular soft tissue swelling on the radial aspect of the second metacarpophalangeal joint (asterisk) which is the typical radiographic appearance of juxta-articular tophus. Adjacent erosions involving the second metacarpal head and the base of the proximal phalanx of the second finger show overhanging margins (arrows). (B) Tophaceous matter (t) is homogeneous and isointense to muscle on the T1-weighted coronal MRI image. (C) A more heterogeneous, intermediate to high signal intensity is appreciable on T2 weighted and (D) short tau inversion recovery (STIR) images.

ure 1). The joint space is relatively well preserved, even in the presence of extensive juxta-articular erosions, and there is a characteristic lack of juxta-articular osteoporosis (1, 3, 6).

Ultrasonography (US)

In the early phase of gouty arthritis, US examination of the affected joints may reveal non-specific findings, such as synovial effusion and mild synovial hypertrophy and hypervascularity, which may also be present in other forms of acute arthritis (2, 3).

A more specific US finding of gout is the presence of a particulate matter inside the synovial fluid with a “snowstorm” appearance, determined by the presence of multiple foci with different echogenicity, which are considered to be MSU crystals within the joint effusion (16, 17). Another specific US feature of gout is the “double contour sign”, represented by an irregular, hyperechoic line which depicts the outer margin of the articular hyaline cartilage and is determined by MSU crystal deposition at the chondro-synovial interface (16, 17). This

feature has also been reported in 17-25% of patients with asymptomatic hyperuricemia (18). In addition, US can be helpful in detecting MSU crystal deposits into tendon sheaths, bursae, subcutaneous and peritendinous soft tissues.

On US images, tophi demonstrate different reflectivity patterns which are related to the grade of compactness of MSU crystal deposits. “Soft” tophi appear as heterogeneously echogenic nodules with internal hyperechoic spots and no posterior acoustic shadowing, while “hard” tophi are composed of heterogeneous hypoechoic material that obstructs the propagation of the US beam (16, 17). The presence of vascularity in and around tophi may be appreciated by applying color- and power-Doppler modules (11, 19).

A promising US-based imaging tool that may be useful in the characterization of gout tophi, and in their differential diagnosis with other subcutaneous nodules, is represented by real-time sonoelastography (20). This US technique investigates the elastic properties of tissues using a color-

coded map (the “elastogram”) which is superimposed on the morphological B-mode image and reflects the different stiffness of adjacent tissues. A recent preliminary study (20) showed that sonoelastography could help distinguish gout tophi from rheumatoid nodules.

US technique offers a radiation-free and real-time guidance to aspirate even minimal joint or bursal effusions for diagnostic purposes, and to deliver anti-inflammatory drugs into the intra-articular space with safe, efficient and non-invasive monitoring of the whole procedure (3, 16, 17, 21).

Computed Tomography (CT) and Dual Energy CT (DECT)

CT is currently considered the reference standard imaging technique for the demon-

stration of cortical bone erosions in inflammatory arthritides (Figure 2). It has been shown to be more sensitive than plain film radiography in the detection of cortical bone erosions associated with tophi, providing direct visualization of tophaceous matter infiltration through these cortical lesions into the subcortical trabecular bone (3, 22). It has been demonstrated that all large gouty erosions detected by CT are characterized by the presence of intraosseous tophi (tophaceous matter extending into the subcortical spongy bone) (3).

Gerster *et al.* demonstrated that tophi have a specific attenuation value ranging from 160 to 200 Hounsfield Units (UH) due to the physical properties of sodium nuclei that are present in MSU crystals (7, 23). The density values of tophi are significantly lower than that of calcium-containing crystal deposits, which are of approximately 450 UH or more (7). The diffuse calcification of tophi is atypical, and it often reflects a coexisting abnormality of calcium metabolism, such as chronic renal insufficiency (19, 24, 25).

DECT is a new imaging technique which employs two X-ray beams with different energy spectra to assess the attenuation differences within a volume of tissue, providing information on its composition using a color-coded map (26). It is an established imaging approach to detect cardiovascular calcifications (27) and it has also been used to characterize uric acid renal stones, differentiating them from other types of renal stones both *in vivo* and *in vitro* (28). DECT is useful to detect and quantify MSU crystals in joint and soft tissues, and for monitoring their reduction in response to hypouricemic therapy. It can differentiate MSU deposits from connective tissues and from calcium containing structures by their X-ray absorption properties.

DECT can identify subclinical tophi, thus representing a valuable tool in the early diagnosis of gout (26-29). Furthermore, DECT scans provide a colour-coded map of the presence and extension of MSU crystal deposits, thus providing a computer automated procedure to measure the volume of each clinical or subclinical tophus and

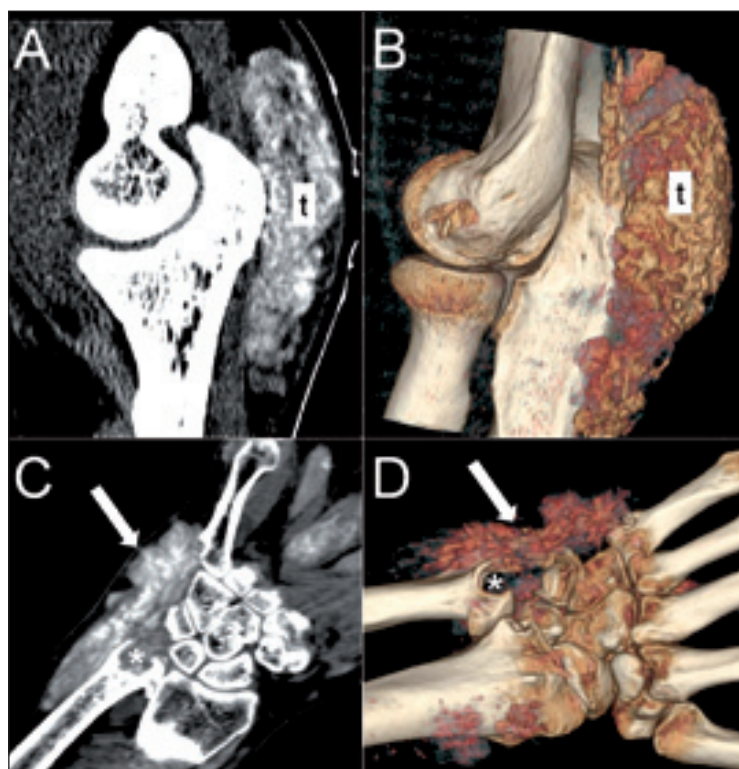


Figure 2 - The (A) sagittal and (B) surface rendered CT reconstructed images show a large tophus (t) in the olecranic bursa. Tophi have a mean attenuation value of approx. 160-200 UH due to the presence of MSU crystals, which is inferior to that of calcium-containing crystals and bone cortex. The (C) coronal and (D) surface rendered CT reconstructed images show an intra-tendineous tophus (large arrow) within the extensor carpi ulnaris tendon and a large erosion in the distal epiphysis of the ulna (asterisk).

the total uric acid volume (26-29). These values can be monitored during patient follow up.

Magnetic Resonance Imaging

MRI is used as primary imaging only in the rare cases of gout involving the spine, or when a solitary tophus, presenting as a soft tissue mass, may be confused with a tumor (7, 9).

In a recent study based on Gadolinium enhanced MRI, (8) a high prevalence of synovitis, erosions and bone marrow edema of the wrist was demonstrated in patients undergoing their first gouty attack in that location. MRI is able to detect small, non-palpable tophaceous deposits and the presence of subclinical erosive alterations before they can be seen on plain film X-ray, demonstrating the typical sparing of hyaline cartilage thickness of the affected joints (30).

The MRI appearance of peripheral tophi in patients with chronic gout has been described using both high-field, total body and low-field, extremity-dedicated MRI systems (5, 7, 30-33). MRI tissue characterization is useful to differentiate tophi from other soft-tissue nodular lesions, especially when they represent the first, unusual manifestation of a chronic asymptomatic hyperuricemia; a condition known as "gout nodulosis" (6, 9, 11).

On T1 weighted MRI images, tophi show a homogeneous intermediate signal intensity, similar to that of muscle (Figure 1). Conversely, on T2 weighted images, a wide spectrum of signal intensity patterns can be observed, ranging from high signal intensity to heterogeneous low signal intensity, thus reflecting their variable composition and relative proportions of MSU crystals, proteins, fibrous tissue, and hemosiderin (5, 9, 11). A homogeneous pattern of contrast enhancement after intravenous administration of paramagnetic contrast media is reported to be more frequent than a heterogeneous enhancement. Peripheral enhancement of the gouty tophi has also been reported (21, 24, 34-37).

Short tau inversion recovery (STIR) and Fast Spin Echo (FSE) T2 weighted se-

quences with fat suppression are able to demonstrate the presence of bone marrow edema that can be variably associated in gout with erosions, synovitis, or the presence of tophi alone (5, 9).

■ CALCIUM PYROPHOSPHATE DIHYDRATE DEPOSITION DISEASE (CPPD)

CPPD crystal deposition disease is a specific term for an osteoarticular disorder characterized by the presence of CPP crystals in or around joints (37). These crystals may elicit an inflammatory response that results in arthritis with joint effusion, synovitis, tenosynovitis or tendonitis. The prevalence of CPP deposition increases with age; it is common in the geriatric population where it is most frequently asymptomatic. X-ray evidence of hyaline and fibrous cartilage calcification is called chondrocalcinosis, which may be a feature of CPPD deposition disease.

However, chondrocalcinosis is not necessarily associated with CPPD arthropathy and it may also occur from the deposition of other calcium-containing crystals, such as calcium apatite, dicalcium phosphate dehydrate, or calcium oxalate (37). The presence of chondrocalcinosis could support, but does not confirm, the diagnosis of CPPD deposition disease.

Clinical presentations of CPP crystal deposition disease are highly variable, including five distinct clinical patterns: lanthanic or asymptomatic, pseudogout syndrome, pseudo-rheumatoid arthritis, pseudo-neuropathic arthropathy, and pseudo-osteoarthritic types. These range from asymptomatic disease to severe painful and destructive arthropathy (37-39). These different patterns are reflected in the corresponding imaging features.

Plain film X-ray

Plain film X-ray plays an important role in the diagnosis of CPP deposition identifying both chondrocalcinosis and periarticular calcifications (Figure 3). CPP crystal deposition in fibrocartilage is most



Figure 3 - Plain film X-rays of different patients demonstrating chondrocalcinosis involving the (A) menisci (large arrows) and (B) the disc of the triangular fibrocartilage complex (large arrow). (C) shows faint intra-articular calcifications (arrows) of the third metacarpophalangeal joint. Joint space narrowing and subchondral bone sclerosis are also present.

commonly observed in the menisci of the knee, triangular fibrocartilage of the wrist, labra of the acetabulum, symphysis pubis and annulus fibrosus of the intervertebral disk. Other less common sites of CPP crystal deposition in cartilage include the articular disks of the sternoclavicular and acromioclavicular joints, and glenoid labra (40, 41).

Hyaline cartilage calcification occurs most commonly in the wrist, knee, elbow, and hip, and is identified on X-ray as a thin line parallel to the subchondral bone.

Calcification within the synovial membrane is a common feature of CPPD deposition disease. It is usually seen with chondrocalcinosis, but it may sometimes be the dominant X-ray feature (37). Synovial calcification is seen most often in the knee, metacarpophalangeal and metatarsophalangeal joints, and the radiocarpal and distal radioulnar joints of the wrist (42). CPP crystal deposition may also involve the fibrous capsule and ligaments. CPP crystal deposition in the scapho-lunate ligament of the carpus may predispose it to rupture with subsequent scapholunate collapse (43). Tendon calcifications are more frequently found in the supraspinatus, triceps, quadriceps, gastrocnemius and Achilles tendons, where they appear as thin and lin-

ear radiodense alterations that extend at a considerable distance from the osseous insertion. They can be distinguished from the more homogeneous, discrete, and nodular calcifications of calcium hydroxyapatite crystal deposition disease (37).

Bursal calcifications are typically amorphous or cloudlike.

Occasionally, CPP calcifications may present in the subcutaneous soft tissue of the fingers, mimicking gout tophi on physical examination and appearing as densely calcified tumor-like collections on X-rays (37). Structural joint changes that are associated with CPP crystal deposition are common and similar to those of osteoarthritis (OA), including joint space narrowing, subchondral sclerosis, and subchondral cyst formation. They are not always accompanied by calcification discernible by X-ray and, in this case, it may be difficult to differentiate regular OA from OA associated with CPPD arthropathy (37).

Ultrasonography (US)

CPP arthropathy has characteristic appearances on US images. Crystal deposition can be identified within hyaline cartilage, fibrocartilage, synovial fluid and synovial membrane. Typical CPP crystal deposits can be visualized as focal hyperechoic spots or

hyperechoic thin bands without a posterior acoustic shadow within the substance of the hyaline cartilage at different anatomical sites, including femoral condyles and metacarpal heads (16). The pattern of crystal deposition of CPP arthropathy is very different from that of gout, where MSU crystal aggregates follow the contour of the chondro-synovial interface. In a recent study, Filippucci et al. detected hyperechoic CPP crystal aggregates within articular cartilage in 69% of patients with CPP arthropathy. These crystals were present in only 2% of controls, resulting in a specificity of 97.6% (16).

Intratendinous crystal deposits appear as hyperechoic spots or bands within the fibrillar echotexture of tendons and may generate a posterior acoustic shadow.

CPP crystal deposits within the fibrocartilage appear as hyperechoic rounded or amorphous-shaped areas and their location can be confirmed by dynamic assessment of the joint during real-time scanning. CPP aggregates can be easily identified by US in the menisci of the knee and in the triangular fibrocartilage of the wrist (44).

Computed Tomography (CT)

CT can accurately demonstrate early chondrocalcinosis and small intra- and periarticular calcifications due to its high spatial resolution. Despite the fact that the role of CT in the assessment of peripheral joint involvement in crystal-induced arthropathies has been little explored, it has been shown

to be particularly useful in the diagnosis of axial involvement, as testified by the so called “crowned dens syndrome” (CDS), a rare presentation of CPP crystal disease (Figure 4) (45, 46). CPP is a clinical-radiological entity that predominantly affects women with mean age 60-70 years at the time of diagnosis. CDS is characterized on X-ray by calcification of the ligaments surrounding the odontoid process of the axis. It is clinically accompanied by acute attacks of cervico-occipital pain, with fever and general signs of inflammation lasting from days to several weeks (46).

In CDS, CT is the gold standard imaging modality because it allows identification of the different X-ray patterns of the disease: simple band of calcification or double band of thin calcifications in the transverse ligament, irregular calcifications crowning the dens apex, bone erosions of the dens itself, fracture, and atlantoaxial subluxation (37).

Magnetic Resonance Imaging (MRI)

Calcific deposits are most typically associated with loss of signal intensity on MRI.

To date, there is no evidence to support the use of MRI in the evaluation of patients with suspected CPP and plain film X-ray has shown greater sensitivity than MRI in the diagnosis of CPP arthropathy of the knee (47). However, MRI does play a role in assessing rare complications of CPP deposition disease, such as spinal cord compression related to large calcified deposits within the spine (48). In fact, CPP may be

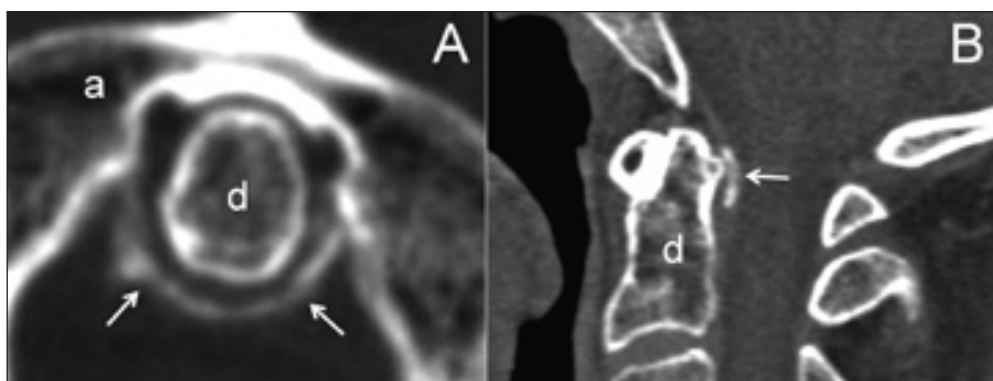


Figure 4 - “Crowned dens” syndrome. (A) Axial CT image demonstrates complete calcification of the transverse ligament of the atlas (arrows) which is also well appreciable on the sagittal CT reconstruction (B). a, atlas; d, dens of the epistropheus.

deposited in both ligamentum flavum and posterior longitudinal ligament, leading to myelopathy, cord compression, and spinal stenosis.

The thoracic and lumbar regions of the spine are often affected, especially at the L2-3 disk level, where MRI may demonstrate low signal intensity CPP crystal deposits in the ligamentum flavum. MRI is also useful for a precise assessment of spinal cord involvement in “crowned dens” syndrome (48).

■ HYDROXYAPATITE DEPOSITION DISEASE (HADD)

Calcium hydroxyapatite crystals can cause typical calcifications of the periarticular soft tissues, mainly tendons at their site of attachment, and bursae (1, 49). The HA crystal deposits may be responsible for an idiopathic disorder called hydroxyapatite deposition disease (HADD), also known as “calcific periarthritis”, “periarticular apatite deposition”, and “calcifying tendinitis” (Figure 5) (50). Usually monoarticular, the disease more frequently involves the shoulder rotator cuff, although other or multiple sites of involvement may occur. Supraspinatus tendon, collateral ligaments of the elbow, triceps tendon at its attach-

ment on the olecranon, gluteal tendon insertions on the greater trochanter and surrounding bursae are the anatomical sites most commonly affected (37, 38, 51).

Deposition of HA crystals may also occur in the axial skeleton (longus colli muscle), pelvis, and thighs. Prevalence among asymptomatic individuals is reported to be 2.7%. When calcifications are present, clinical symptoms occur in 34 to 45% of patients (52). The disease typically occurs between the ages of 40 and 70 years, with no gender predilection; a familial predisposition has also been suggested (53). The onset of symptoms in HADD is typically acute, with severe pain, tenderness, signs of local inflammation and functional limitation (37, 54).

In the shoulder, calcific tendinitis of the rotator cuff is regarded as a self-healing condition that usually undergoes spontaneous resolution in 7-10 days. It can, however, be disabling and pain may be resistant to conservative treatment with local steroid injections and anti-inflammatory compounds. Although etiology remains unknown, HADD is recognized as a dynamic process that evolves through four stages: precalcific, calcific, resorptive, and postcalcific. In the first stage, microtraumatic factors, associated to a local decrease in blood supply, can lead to intratendinous

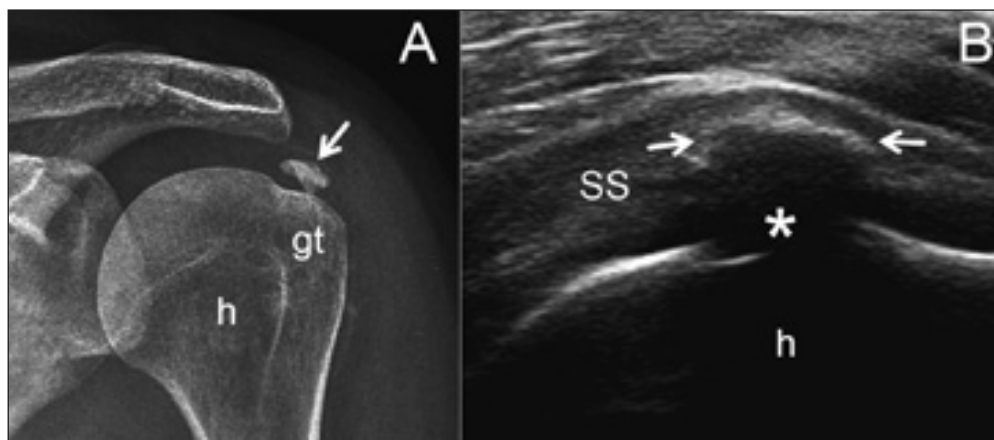


Figure 5 - Type I calcification of the supraspinatus tendon. (A) Plain film X-ray shows a dense, homogeneous oval opacity (arrow) with sharply defined margins above the greater tuberosity of the humeral head. (B) US longitudinal scan demonstrates the pre-insertional calcification of the supraspinatus tendon (SS) as a well-defined hyperechoic lesion (arrows) with posterior acoustic shadowing (asterisk). h, humeral head; gt, greater tuberosity.

fibrocartilaginous metaplasia with resulting calcification (55-59). In the shoulder, this condition is typically associated with an intact rotator cuff. The subsequent calcific phase is a resting period which can sometimes be painful or may cause mechanical symptoms, according to the size of the deposit (60). The resorptive stage is frequently symptomatic, and is characterized by vascular proliferation followed by dissolution and resorption of the calcific focus by macrophages, resulting in a "toothpaste" appearance of the calcific deposit. When this ruptures, HA crystals are spilled into the surrounding soft tissues or bursa, setting off the acute inflammatory response with very intense pain. An association between acute pain attacks and histological evidence of calcium resorption has been described (58, 61). After resorption, in the postcalcific or reparative phase, fibroblasts restore the normal tendineous collagen pattern (60).

The intra-articular location of HA crystals is also found as a primary phenomenon or in association with other disorders, including trauma, renal osteodystrophy, collagen vascular disease, tumoral calcinosis and as a complication of multiple intra-articular steroid injections (62).

X-ray

X-ray is the most practical, cost-effective and available imaging modality for evaluating HA crystals deposition disorder. HADD may present on X-ray as a cloud-like and poorly defined clump of calcifications in periarticular soft tissues (Figure 5). The HA deposits with these characteristics are classified as type III calcifications according to Gartner (63, 64). Type I calcifications are more dense and homogeneous with sharply defined margins and a linear or circular configuration. In some cases it is not possible to designate the specific X-ray morphology to a given deposit (type II). A typical feature helping the differential diagnosis from heterotopic ossification or accessory ossicles is the complete lack of trabeculation in the HA crystals opacities (65).

Deposits may remain static over the years

or they can also enlarge, change shape, or disappear. The adjacent osseous tissues are usually normal, but osteoporosis, subchondral cystic lesions, reactive sclerosis, and contour bone irregularities may also be present (1).

Calcified deposits with a well-defined, homogeneous contour are less likely to be symptomatic and may correlate with the formative or calcific phase of the disease. On the other hand, deposits with fluffy, ill-defined edges are often seen in patients with acute pain and may correlate with the resorptive phase (66). It is important to point out that HA crystal deposition may often be associated with osteoarthritis, and the radiographic feature of one disease may accompany the other.

HA crystal deposits in the subacromial bursa result in a teardrop-shaped radiodensity extending under the greater tuberosity. In rare cases, HA crystal deposition in the glenohumeral joint can be associated with destructive arthropathy, referred to as Milwaukee shoulder syndrome, which is characterized by joint space loss, subchondral sclerosis, osseous debris, and joint deformity (65, 67, 68). A large effusion that contains calcified debris may be present, as well as the superior displacement of the humeral head as a result of associated disruption of the rotator cuff with remodeling and erosion of the acromial undersurface.

Ultrasound

Ultrasound (US) is a useful tool in the evaluation of HADD (61, 69), particularly when it affects the shoulder rotator cuff, providing a real-time, high-resolution analysis of tendinous echostructure (Figure 5). Moreover, it can guide mini-invasive therapeutic procedures (i.e. single or double needle lavage techniques, intra-articular injection of anti-inflammatory drugs) with real-time visualization (61, 69, 70). Three types of calcifications have been described by Farin et al. (71): type I consists of a hyperreflexive lesion with a well-circumscribed dorsal acoustic shadow; type II deposits are well circumscribed, homogeneous hyper-echoic foci with a faint posterior shadow; type III are amorphous, unhomogeneous

hyperechoic foci without posterior acoustic shadow. Consistence is solid for deposits of types I and II and semiliquid for type III. Large and slurry calcifications and bursal calcifications are better seen on US images, but plain X-ray is more useful for small and more scattered deposits.

Computed Tomography

CT imaging is highly accurate in predicting the consistency of HA crystal deposits in relation to their mean attenuation value. HA crystal deposits with a well-defined X-ray appearance are generally homogeneous on CT images, while soft and semiliquid calcifications tend to have a heterogeneous appearance (72). The mean density for the unhomogeneous and amorphous calcifications is reported to be 166 HU (range 132-288 HU) while homogeneous and well-defined calcifications have a mean attenuation value of 476 HU (range 333-945 HU) (72). In addition, CT can accurately depict cortical pseudocysts and irregularities in HADD patients who do not show any cortical defect on plain film X-ray (73).

Magnetic Resonance

Although MR imaging is not sufficient to diagnose calcific tendinitis (74), it is an important tool in the evaluation of HADD, and can help analyze the extent of the HA crystal deposits, visualizing soft tissue abnormalities, and helping to exclude other causes of joint pain (73). Unfortunately, small calcific deposits may be difficult to visualize and lead to false-negative results; similarly, normal hypointense areas within tendons may lead to false-positive results (74).

Calcific deposits are typically associated with focal signal intensity loss on MR images, because at high calcium concentrations (above 30-40%) susceptibility effects and low proton density lead to a loss of signal intensity (75). At lower concentrations of calcium, T1 shortening effects dominate, resulting in isointensity or even hyperintensity of HA crystal deposits (75). High-contrast, fluid sensitive MR sequences (Fast Spin Echo T2 weighted with or without fat suppression, short tau inversion recovery; STIR) may demonstrate soft tis-

sue edema surrounding HA crystal deposits and adjoining bone marrow edema.

■ CONCLUSIONS

Plain film X-ray is inexpensive and widely available. It is, therefore, considered the first-step imaging approach in the assessment of crystal-induced arthropathies. It provides specific findings for both CPPD and HADD, but it may underdiagnose the early osteoarticular damage in gouty patients. High-resolution US has several advantages in clinical practice when compared to other imaging modalities due to the lack of ionizing radiations, low cost, acceptability by the patient and ease of access. Several specific US findings are useful in the diagnosis of crystal deposition diseases. However, this is operator-dependent and labour-intensive, and standardization of images for a precise assessment of lesions over time may be difficult. In addition, US does not provide a panoramic view of the affected joint and surrounding soft tissues and is unable to detect pathological changes in the subchondral/subcortical bone; for these reasons US should always be associated with X-rays and/or other imaging techniques for a comprehensive assessment of the osteoarticular damage. CT can provide high-resolution images of crystal deposits which are characterized by different and almost specific attenuation values. DECT is a promising imaging approach in the assessment of subclinical gout but for the moment, this new CT-based technique is only available in a few centers. The main disadvantages of CT are the use of ionizing radiation, its relatively high cost and the low contrast resolution. MRI is of extremely useful in the evaluation of both acute and chronic gout in both the acute and chronic settings. The high costs and limited availability of high-field total body MRI scanners restrict its use. Low-field, extremity-dedicated MRI systems have been recently used to assess acute gouty arthritis and chronic tophaceous gout, giving encouraging results.

■ REFERENCES

- Choi MH, John D, MacKenzie, Murray K, Dalinka. Imaging features of crystal-induced arthropathy. *Rheum Dis Clin N Am* 2006; 32: 427-46.
- Rosenberg AE. Crystal arthropathies. In: Coltran RS, Kumar V, Robbins SL, Schoen FJ, editors. *Robbins' pathologic basis of disease*. 5th edition. Philadelphia: WB Saunders; 1994; 1255-8.
- Dalbeth N, McQueen FM. Use of imaging to evaluate gout and other crystal deposition disorders. *Curr Opin Rheumatol* 2009; 21: 124-31.
- Wortmann RL. Gout and hyperuricemia. In: Firestein G, ed. *Kelley's Textbook of Rheumatology*. Philadelphia: Saunders Elsevier, 2008; 1481-524.
- Yu JS, Chung C, Recht M, Dailiana T, Jurdi R. MR imaging of tophaceous gout. *Am J Roentgenol* 1997; 168: 523-7.
- Monu JUV, Pope TL, JR. Gout: a clinical and radiologic review. *Radiol Clin N Am* 2004; 42: 169-84.
- Gerster JC, Landry M, Dufresne L, Meuwly JY. Imaging of tophaceous gout: computed tomography provides specific images compared with magnetic resonance imaging and ultrasonography. *Ann Rheum Dis* 2002; 61: 52-4.
- Cimmino MA, Zampogna G, Parodi M, Andracco R, Barbieri F, Paparo F, Ferrero G, Garlaschi G. MRI synovitis and bone lesions are common in acute gouty arthritis of the wrist even during the first attack. *Ann Rheum Dis* 2011; 70: 2238-9.
- Paparo F, Zampogna G, Fabbro E, Parodi M, Andracco R, Ferrero G, Garlaschi G, Cimmino MA. Imaging of tophi with an extremity-dedicated MRI system. *Clin Exp Rheumatol* 2011; 29: 519-26.
- Paul H, Reginato AJ, Schumacher HR. Alizarin red S staining as a screening test to detect calcium compounds in synovial fluid. *Arthritis Rheum* 1983; 26: 191-200.
- Gentili A. The advanced imaging of gouty tophi. *Curr Rheumatol Rep* 2006; 8: 231-5.
- Wallace SL, Robinson H, Masi AT, et al. Preliminary criteria for the classification of the acute arthritis of primary gout. *Arthritis Rheum* 1977; 20: 895-900.
- Dalbeth N, Clark B, McQueen F, Doyle A, Taylor W. Validation of a radiographic damage index in chronic gout. *Arthritis Rheum* 2007; 57: 1067-73.
- Van der Heijde D. How to read radiographs according to the Sharp/van der Heijde method. *J Rheumatol* 2000; 27: 261-3.
- Martel W. The overhanging margin of bone: a roentgenologic manifestation of gout. *Radiology* 1968; 91: 755-6.
- Grassi W, Meenagh G, Pascual E, Filippucci E. "Crystal clear" - sonographic assessment of gout and calcium pyrophosphate deposition disease. *Semin Arthritis Rheum* 2006; 36: 197-202.
- Gutierrez M, Filippucci E, Salaffi F, Grassi W. The current role of ultrasound in the assessment of crystal related arthropathies. *Reumatismo* 2009; 61: 216-21.
- Pineda C, Amezcua-Guerra LM, Solano C, Rodriguez-Henrriquez P, Hernández-Díaz C, Vargas A, Hofmann F, Gutiérrez M. Joint and tendon subclinical involvement suggestive of gouty arthritis in asymptomatic hyperuricemia: an ultrasound controlled study. *Arthritis Res Ther* 2011; 13: R4.
- Paparo F, Sconfienza LM, Muda A, Denegri A, Piccazzo R, Aleo E, Cimmino MA. Multimodality imaging of chronic tophaceous gout. *Reumatismo* 2010; 62: 286-91.
- Sconfienza LM, Silvestri E, Bartolini B, Garlaschi G, Cimmino MA. Sonoelastography may help in the differential diagnosis between rheumatoid nodules and tophi. *Clin Exp Rheumatol* 2010; 28: 144-5.
- Perez-Ruiz F, Dalbeth N, Urresola A, de Miguel E, Schlesinger N. Imaging of gout: findings and utility. *Arthritis Res Ther* 2009; 11 (3): 232.
- Møller Døhn U, Ejbjerg Bo J, Hasselquist M, Narvestad E, Møller J, Thomsen HS, et al. Detection of bone erosions in rheumatoid arthritis wrist joints with magnetic resonance imaging, computed tomography and radiography. *Arthritis Res Ther* 2008; 10: R25.
- Gerster JC, Landry M, Duvoisin B, Rappoport G. Computed tomography of the knee joint as an indicator of intraarticular tophi in gout. *Arthritis Rheum* 1996; 39: 1406-9.
- Lioté F, Ea HK. Gout: update on some pathogenic and clinical aspects. *Rheum Dis Clin North Am* 2006; 32: 295-311, vi.
- Paparo F, Ameri P, Denegri A, Revelli M, Muda A, Garlaschi G, Cimmino MA. Multimodal imaging in the differential diagnosis of soft tissue calcinosis. *Reumatismo* 2011; 63: 175-184.
- Choi HK, Al-Arfaj AM, Eftekhari A, Munk PL, Shojania K, Reid G, Nicolaou S. Dual energy computed tomography in tophaceous gout. *Ann Rheum Dis* 2009; 68: 1609-12.
- Johnson TR, Weckbach S, Kellner H, Reiser MF, Becker CR. Clinical image: dual-energy computed tomographic molecular imaging of gout. *Arthritis Rheum* 2007; 56: 2809.
- Reimann AJ, Rinck D, Birinci-Aydogan A, et al. Dual-source computed tomography: advances of improved temporal resolution in coronary plaque imaging. *Invest Radiol* 2007; 42: 196-203.
- Graser A, Johnson TR, Bader M, et al. Dual energy CT characterization of urinary calculi: initial in vitro and clinical experience. *Invest Radiol* 2008; 43: 112-9.

30. Popp JD, Bidgood WD Jr, Edwards LN. Magnetic resonance imaging of tophaceous gout in the hands and wrists. *Semin Arthritis Rheum* 1996; 25: 282-9.
31. Schumacher HR Jr, Becker MA, Edwards NL, Palmer WE, MacDonald PA, Palo W, Joseph-Ridge N. Magnetic resonance imaging in the quantitative assessment of gouty tophi. *Int J Clin Pract* 2006; 60: 408-14.
32. Chen CK, Chung CB, Yeh L, Pan HB, Yang CF, Lai PH, Liang HL, Resnick D. Carpal tunnel syndrome caused by tophaceous gout: CT and MR imaging features in 20 patients. *Am J Roentgenol* 2000; 175: 655-9.
33. Chen CK, Yeh LR, Pan HB, Yang CF, Lu YC, Wang JS, Resnick D. Intra-articular gouty tophi of the knee: CT and MR imaging in 12 patients. *Skeletal Radiol* 1999; 28: 75-80.
34. Dalbeth N, Clark B, Gregory K, Gamble G, Sheehan T, Doyle A, McQueen FM. Mechanisms of bone erosion in gout: a quantitative analysis using plain radiography and computed tomography. *Ann Rheum Dis* 2009; 68: 1290-5.
35. Dalbeth N, Smith T, Nicolson B, Clark B, Callon K, Naot D, Haskard DO, McQueen FM, Reid IR, Cornish J. Enhanced osteoclastogenesis in patients with tophaceous gout: urate crystals promote osteoclast development through interactions with stromal cells. *Arthritis Rheum* 2008; 58: 1854-65.
36. Sainsbury DC, Hidvegi N, Blair JW. Intra-tendinous gout in a repaired flexor digitorum profundus. *J Hand Surg Eur Vol* 2008; 33: 528-9.
37. Steinbach LS. Calcium pyrophosphate dihydrate and calcium hydroxyapatite crystal deposition diseases: imaging perspectives. *Radiol Clin North Am* 2004; 42: 185-205, vii.
38. Richards AJ, Hamilton EBD. Destructive arthropathy in chondrocalcinosis articularis. *Ann Rheum Dis* 1973; 33: 196-203.
39. Resnick D, Niwayama G, Georgen TG, et al. Clinical, radiographic and pathologic abnormalities in calcium pyrophosphate dihydrate deposition disease (CPPD): pseudogout. *Radiology* 1977; 122: 1-15.
40. Huang GS, Bachmann D, Taylor JAM, et al. Calcium pyrophosphate dihydrate crystal deposition disease and pseudogout of the acromioclavicular joint: radiographic and pathologic features. *J Rheumatol* 1993; 20: 2077-82.
41. Cooper AM, Hayward C, Williams BD. Calcium pyrophosphate deposition disease: involvement of the acromioclavicular joint with pseudocyst formation. *Br J Rheumatol* 1993; 32: 248-50.
42. Shumacher HR. Ultrastructural findings in chondrocalcinosis and pseudogout. *Arthritis Rheum* 1976; 19 (Suppl): 413-25.
43. Doherty W, Lovallo JL. Scapholunate advanced collapse pattern of arthritis in calcium pyrophosphate deposition disease of the wrist. *J Hand Surg* 1993; 18A: 1095-8.
44. Ciapetti A, Filippucci E, Gutierrez M, Grassi W. Calcium pyrophosphate dihydrate crystal deposition disease: sonographic findings. *Clin Rheumatol* 2009; 28: 271-6.
45. Bouvet JP, le Parc JM, Michalski B, et al. Acute neck pain due to calcifications surrounding the odontoid process: the crowned dens syndrome. *Arthritis Rheum* 1985; 28: 1417-20.
46. Scutellari PN, Galeotti R, Leprotti S, et al. The crowned dens syndrome. Evaluation with CT imaging. *Radiol Med* 2007; 112: 195-207.
47. Abreu M, Johnson K, Chung CB, et al. Calcification in calcium pyrophosphate dihydrate (CPPD) crystalline deposits in the knee: anatomic, radiographic, MR imaging, and histologic study in cadavers. *Skeletal Radiol* 2004; 33: 392-8.
48. Fenoy AJ, Menezes AH, Donovan KA, Kralik SF. Calcium pyrophosphate dihydrate crystal deposition in the craniovertebral junction. *J Neurosurg Spine* 2008; 8: 22-9.
49. McCarty Jr DJ, Gatter RA. Recurrent acute inflammation associated with focal apatite crystal deposition. *Arthritis Rheum* 1966; 9: 804-19.
50. Faure G, Daculsi G. Calcified tendinitis: a review. *Ann Rheum Dis* 1983; 42 (Suppl 1): 49-53.
51. Lam F, Bhatia D, van Rooyen K, de Beer JF. Modern management of calcifying tendinitis of the shoulder. *Curr Orthopaed* 2006; 20: 446-52.
52. Uthoff HK. Anatomopathology of calcifying tendinitis of the cuff. In: Gazielly DF, Gleyze PTT, editors. *The cuff*. Paris: Elsevier; 1997; 144-6.
53. Amor B, Cherot A, Delbarre F, et al. Hydroxyapatite rheumatism and HLA markers. *J Rheumatol Suppl* 1977; 3: 101-4.
54. Selby CL. Acute calcific tendinitis of the hand: an infrequently recognized and frequently misdiagnosed form of periartthritis. *Arthritis Rheum* 1984; 27: 337-40.
55. Speed CA, Hazleman BL. Calcific tendinitis of the shoulder. *N Engl J Med* 1999; 340: 1582-84.
56. Bosworth BM. Calcium deposits in the shoulder and subacromial bursitis: a survey of 12,122 shoulders. *JAMA* 1941; 116: 2477-82.
57. Bianchi S, Martinoli C. Shoulder. In: Bianchi S, Martinoli C, eds. *Ultrasound of the musculoskeletal system*. Berlin, Germany: Springer-Verlag, 2007; 190-331.
58. Uthoff HK, Sarkar K. Calcifying tendonitis. *Baillieres Clin Rheum* 1989; 3: 567-581.
59. Hurt G, Baker CL Jr. Calcific tendinitis of the shoulder. *Orthop Clin North Am* 2003; 34: 567-75.
60. Uthoff HK, Loehr JW. Calcific tendinopathy

- of the rotator cuff: pathogenesis, diagnosis, and management. *J Am Acad Orthop Surg* 1997; 5: 183-91.
61. Serafini G, Sconfienza LM, Lacelli F, Silvestri E, Aliprandi A, Sardanelli F. Rotator cuff calcific tendonitis: short-term and 10-year outcomes after two-needle US-guided percutaneous treatment - nonrandomized controlled trial. *Radiology* 2009; 252: 157-64.
 62. Dalinka MK, Stewart V, Bomalaski JS, et al. Periarticular calcifications in association with intraarticular corticosteroid injections. *Radiology* 1984; 153: 615-8.
 63. Gärtner J, Heyer A. Calcific tendinitis of the shoulder. *Orthopaede* 1995; 24: 284-302.
 64. Gärtner J, Simons B. Analysis of calcific deposits in calcifying tendinitis. *Clin Orthop Relat Res* 1990; 254: 111-20.
 65. Hayes CW, Conway WF. Calcium hydroxyapatite deposition disease. *Radiographics* 1990; 10: 1031-48.
 66. Vigario GD, Keats TE. Localization of calcific deposits in the shoulder. *Am J Roentgenol Radium Ther Nucl Med* 1970; 108: 806-11.
 67. Halverson PB, McCarty DJ, Cheung HS, et al. Milwaukee shoulder syndrome: eleven additional cases with involvement of the knee in seven (basic calcium phosphate crystal deposition disease). *Semin Arthritis Rheum* 1984; 14: 36-44.
 68. Dieppe PA, Doherty M, MacFarlane DG, et al. Apatite associated destructive arthritis. *Br J Rheumatol* 1984; 23: 84-91.
 69. Aina R, Cardinal E, Bureau NJ, Aubin B, Brassard P. Calcific shoulder tendinitis: treatment with modified US-guided fine-needle technique. *Radiology* 2001; 221: 455-61.
 70. Farin PU, Jaroma H, Soimakallio S. Rotator cuff calcifications: treatment with US-guided technique. *Radiology* 1995; 195: 841-3.
 71. Farin PU, Jaroma H. Sonographic findings of rotator cuff calcifications. *J Ultrasound Med* 1995; 14: 7-14.
 72. Farin PU. Consistency of rotator-cuff calcifications. Observations on plain radiography, sonography, computed tomography, and at needle treatment. *Invest Radiol* 1996; 31: 300-4.
 73. Flemming DJ, Murphey MD, Shekitka KM, Temple HT, Jelinek JJ, Kransdorf MJ. Osseous involvement in calcific tendinitis: a retrospective review of 50 cases. *Am J Roentgenol* 2003; 181: 965-72.
 74. Zubler C, Mengiardi B, Schmid MR, Hodler J, Jost B, Pfirrmann CW. MR arthrography in calcific tendinitis of the shoulder: diagnostic performance and pitfalls. *Eur Radiol* 2007; 17: 1603-10.
 75. Henkelman RM, Watts JF, Kucharczyk W. High signal intensity in MR images of calcified brain tissue. *Radiology* 1991; 179: 199-206.